Article:
Jenkins, Sarah, Chantrell, Roy W., Klemmer, Timothy J. et al. (2019) Magnetic anisotropy of the noncollinear antiferromagnet IrMn3. Physical Review B. 220405(R). ISSN: 2469-9969

https://doi.org/10.1103/PhysRevB.100.220405

Rapid Communications

Magnetic anisotropy of the noncollinear antiferromagnet $IrMn_3$

Sarah Jenkins,[1,*] Roy W. Chantrell,[1,†] Timothy J. Klemmer,[2] and Richard F. L. Evans[1,‡]
[1]*Department of Physics, The University of York, York, YO10 5DD, United Kingdom*
[2]*Seagate Research, Fremont, California 94538, USA*

(Received 28 May 2019; revised manuscript received 19 August 2019; published 11 December 2019)

The magnetic anisotropy of antiferromagnets plays a crucial role in stabilizing the magnetization of many spintronic devices. In noncollinear antiferromagnets such as IrMn, the symmetry and temperature dependence of the effective anisotropy are poorly understood. Theoretical calculations and experimental measurements of the effective anisotropy constant for IrMn differ by two orders of magnitude, while the symmetry has been inferred as uniaxial in contradiction to the assumed relationship between crystallographic symmetry and temperature dependence of the anisotropy from the Callen-Callen law. In this Rapid Communication, we determine the effective anisotropy energy surface of $L1_2$- $IrMn_3$ using an atomistic spin model and constrained Monte Carlo simulations. We find a unique cubiclike symmetry of the anisotropy not seen in ferromagnets and that metastable spin structures lower the overall energy barrier to a tenth of that estimated from simple geometrical considerations, removing the discrepancy between experiment and theory. The temperature scaling of the anisotropy energy barrier shows an exponent of 3.92, close to a uniaxial exponent of 3. Our results demonstrate the importance of noncollinear spin states on the thermal stability of antiferromagnets with consequences for the practical application of antiferromagnets in devices operating at elevated temperatures.

DOI: 10.1103/PhysRevB.100.220405

I. INTRODUCTION

The magnetic anisotropy of antiferromagnetic (AF) materials plays a key role in the stability of many spintronic devices [1–5] and exchange bias effects [6–8]. Recently, interest in the properties of AF materials has increased due to their emerging applications in AF spintronic [3,5] and neuromorphic computing devices [9] where the antiferromagnet is the active element. The magnetic anisotropy energy density as determined experimentally is a free-energy difference between maximum and minimum on the free-energy surface where the temperature variation of the anisotropy arises from spin fluctuations. For clarity, we refer to the intrinsic quantity, determined from *ab initio* calculations, as the magnetocrystalline anisotropy energy (MAE) and the experimental temperature-dependent free-energy density as the magnetocrystalline anisotropy constant K. Magnetic anisotropy is usually classified by symmetry in expansions of spherical harmonics with azimuthal and rotational components [10] describing uniaxial and cubic forms of the anisotropy. The temperature dependence of the anisotropy is intrinsically related to the order of the harmonics [10,11] and is well understood for ferromagnets. In contrast, the magnetic anisotropy of antiferromagnets is poorly understood due to the difficulty in experimental measurements, the complexity of the materials, and noncollinear magnetic structure.

Iridium manganese (IrMn) is the material chosen for many AF spintronic devices due to its high thermal stability and large exchange bias field. In devices, the ordering and composition is tuned for optimal performance but here we focus on the $L1_2$ ordered $IrMn_3$ phase due to the existence of extensive experimental [12,13] and theoretical [14–16] data. Theoretical calculations by Szunyogh *et al.* [14] found an extremely large second-order MAE for $IrMn_3$, leading to a predicted magnetocrystalline anisotropy energy density of the order of 3×10^7 J/m^3 at 0 K. Vallejo-Fernandez *et al.* [17,19] calculated a value of the anisotropy constant $K = 6.2 \times 10^5$ J/m^3 at 300 K or $K = 14.8 \times 10^5$ J/m^3 at 0 K, almost two orders of magnitude lower than the expected value from theoretical calculations [14]. The experimental estimate of the anisotropy constant of IrMn is sensitive to the value of the switching attempt frequency (f_0) in the Arrhenius Néel law given by

$$1/\tau = f_0 \exp\left(-\frac{\Delta E}{k_B T}\right), \tag{1}$$

where τ is the relaxation time, ΔE is the energy barrier, k_B is the Boltzmann constant, and T is the temperature. Originally, Vallejo-Fernandez *et al.* used a value of $f_0 = 10^9$ s^{-1} [17] but more recent estimates suggest values closer to $f_0 = (2.1 \pm 0.4)10^{12}$ s^{-1} [19]. Determination of the exact value of the attempt frequency is therefore critical to determining the effective anisotropy in AF materials.

A further unresolved problem relates to the symmetry of the $IrMn_3$ anisotropy. Vallejo-Fernandez [17] and Craig *et al.* [20] calculated the anisotropy by fitting to the temperature dependence of the magnetization using a Callen-Callen [11] power law $K_{AF}(T)/K_{AF}(0) = (n_{AF}(T)/n_{AF}(0))^l$, with n_{AF} the AF sublattice magnetization. The exponent l reflects the symmetry of the anisotropy, which itself generally reflects that of the lattice. Agreement with experimental measurements [17] requires an exponent of $l \sim 3$ (uniaxial) rather than

*sarah.jenkins@york.ac.uk
†roy.chantrell@york.ac.uk
‡richard.evans@york.ac.uk

$l \sim 10$ (cubic anisotropy). Szunyogh *et al.* [14] showed that the local energy surface for individual spins is uniaxial by rotating the triangular ground state about the (111) direction. Both experiment and theory agree that the anisotropy has an approximately uniaxial form. However, this contradicts the predicted relationship between crystallographic symmetry and the temperature dependence of the anisotropy from the Callen-Callen and Zener relations [10,11].

In this Rapid Communication, we resolve this apparent contradiction by determining the equilibrium anisotropic free-energy surface and by calculation of the temperature dependence and scaling of the effective anisotropy. We find that the anisotropy of $IrMn_3$ possesses a unique symmetry neither uniaxial nor cubic in nature and has an unusual scaling exponent of $l = 3.92$, not seen for ferromagnetic materials.

II. METHOD

To study the anisotropy of $L1_2$- $IrMn_3$ we use an atomistic spin model where the energy of the system is defined using the spin Hamiltonian

$$\mathscr{H} = -\sum_{i<j} J_{ij}\mathbf{S}_i \cdot \mathbf{S}_j - \frac{k_N}{2}\sum_{i\neq j}^{z}(\mathbf{S}_i \cdot \mathbf{e}_{ij})^2, \qquad (2)$$

where $\mathbf{S}_i$ is a unit vector describing the spin direction on Mn site i, $k_N = -4.22 \times 10^{-22}$ is the Néel anisotropy constant, and $\mathbf{e}_{ij}$ is a unit vector from site i to site j, z is the number of nearest neighbors and J_{ij} is the exchange interaction. The effective exchange interactions (J_{ij}) were limited to nearest ($J_{ij}^{\mathrm{nn}} = -6.4 \times 10^{-21}$ J/link) and next-nearest ($J_{ij}^{\mathrm{nnn}} = 5.1 \times 10^{-21}$ J/link) neighbors [21]. In IrMn, the magnetocrystalline anisotropy arises from the large spin-orbit coupling between Mn and Ir sites [14]. Here we map the local anisotropies at each Mn site to a Néel pair anisotropy model [21,22] which gives exact agreement with the *ab initio* calculations [14]. The Néel model reflects the local site symmetry to give the correct easy axes for each Mn site and by performing coherent spin rotations as in Ref. [14], we find the same angular dependence of the anisotropy energy.

III. RESULTS

To verify the model we calculated the ground-state spin structure of ordered $L1_2$ $IrMn_3$ using a Monte Carlo metropolis algorithm with the adaptive update method [23,24] and implemented in the VAMPIRE software package [25]. The $8 \times 8 \times 8$ nm^3 system was initially equilibrated at a temperature of 1500 K (above the Néel temperature) to thermalize the spins. The system was then cooled to 0 K using a linear cooling function over 10^6 Monte Carlo steps to find the ground-state spin configuration. In agreement with previous experimental [12,13] and *ab initio* results [14], we find that ordered $L1_2$-$IrMn_3$ has a triangular ($T1$) spin structure where the magnetic moments lie parallel to the [111] planes as shown in Fig. 1. There are eight [111] planes and, by symmetry, IrMn has eight magnetic ground states.

The energy barrier separating two ground states is the minimum energy path for the spins to rotate between them and defines the effective anisotropy and the thermal stability.

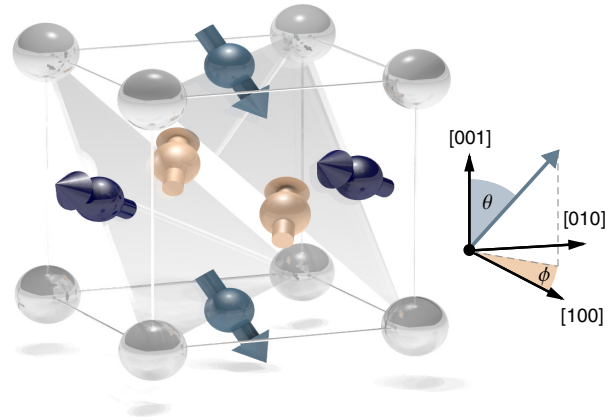

FIG. 1. Visualization of the simulated ground-state spin structure of $L1_2$-$IrMn_3$ obtained from zero-field cooling. The spin directions show an average spin of each magnetic sublattice direction over the whole sample. The corner atoms represent Ir and so have no net magnetic moment. The simulated spin structure agrees with experimental measurements [12,13] and first-principles simulations [14]. Crystallographic directions and reference directions for constraint angles (θ, ϕ) for the sublattice magnetization are shown inset.

To calculate the energy barrier, we use the constrained Monte Carlo algorithm to determine the free-energy surface and the energy barrier to magnetic reversal [26]. Here, we constrain the direction of magnetization of a single Mn sublattice while allowing all other spins to relax to obtain the equilibrium spin structure with a constraint applied. By scanning all angles (θ, ϕ), the energy surface is obtained. For each value of θ and ϕ, the $(8\ \mathrm{nm})^3$ system was initially heated to 1500 K to thermalize the spins and then cooled to 0 K. Due to the constraint, the system cannot reach a full equilibrium and so the total internal torque (τ) is nonzero and given by

$$\tau = -\mathbf{M} \times \frac{\partial \mathscr{F}}{\partial \mathbf{M}}, \qquad (3)$$

where $\mathscr{F}$ is the Helmholtz free energy which is a function of $\mathbf{M}$. Since $\mathscr{F}$ cannot be computed directly, we reconstruct it by numerical integration of the torque

$$\mathscr{F} = \mathscr{F}_0 + \int_M^{M'} (\mathbf{M}' \times \mathbf{T}) \cdot d\mathbf{M}' \qquad (4)$$

taken along any path between two points on the energy surface. The computed energy surface at 0 K is shown in Fig. 2(a) and has a complicated structure with four minima. The energy minima lie at $\phi \sim \pm 56^\circ$, corresponding to the expected easy directions of the constrained sublattice. To calculate the energy barrier between two adjacent minima, we compute the minimum energy path between them as shown in Fig. 2(b). The calculated 0 K anisotropy is 1.78×10^6 J/m^3, which is an order of magnitude lower than that for rigid rotation of spins calculated by Szunyogh *et al.* [14] and has massively reduced the disparity between the experiment and theory with this result being less than 10% off the experimental measurement. The surprising reduction arises due to a bobbing motion of the unconstrained spins which results from the competition between the exchange and anisotropy

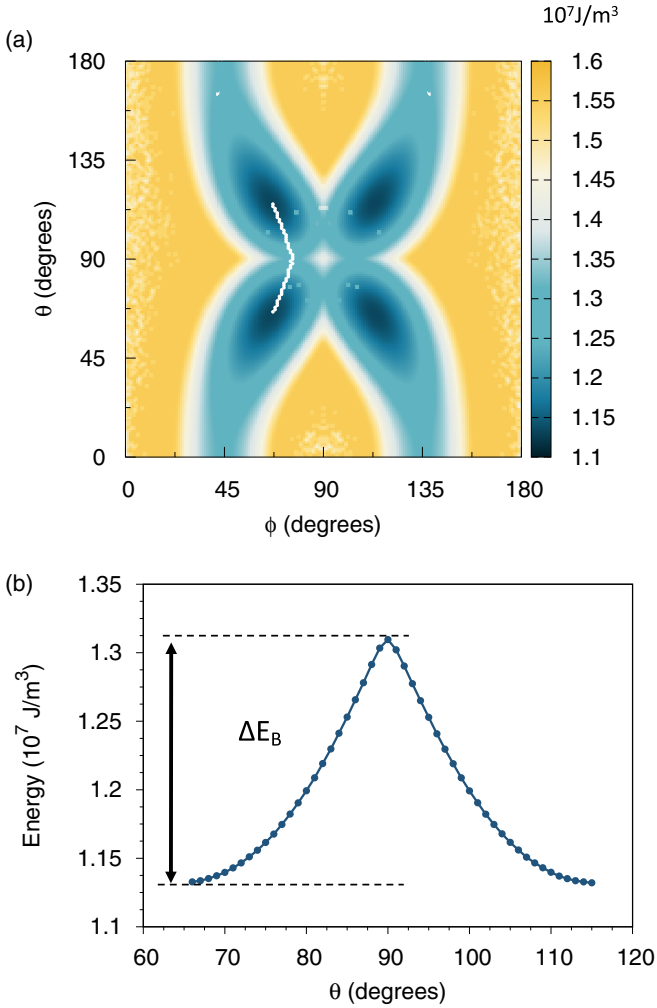

FIG. 2. (a) Simulated anisotropy energy surface for ordered $L1_2$-$IrMn_3$ at 0 K recovered from the integral of the total torque given by Eq. (4). The marked path shows the minimum energy route between the two energy minima. (b) Cross section of the anisotropy surface at $T = 0$ K showing the minimum energy path to reversal. The energy barrier ΔE_B to move between the minima is shown.

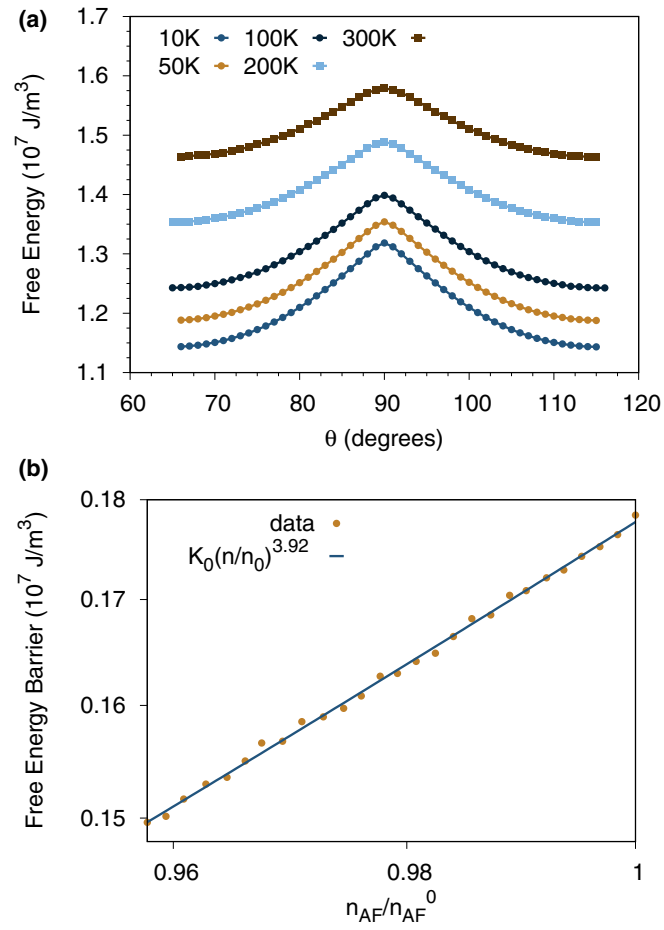

FIG. 3. Simulated temperature dependence of the energy barrier and scaling of the effective anisotropy. (a) The cross-sectional energy surface along the minimum energy path at different temperatures. The total anisotropy energy increases due to spin fluctuations, but the free-energy barrier decreases with temperature. (b) The scaling of the effective energy barrier with sublattice magnetization length n_{AF} fitted using $E_B(n_{AF}) = E_0 n_{AF}^l$. l is calculated to be 3.92, ±0.14 suggesting a scaling similar to uniaxial anisotropy $l = 3$.

energies leading to small deviations from the ground-state spin structure when the AF spins are rotated. This is particularly relevant to macroscopic approximations of AF materials with Néel vectors where the sublattices are always assumed to have a fixed local spin structure. The remaining difference in the values of the effective magnetic anisotropy could be due to different ordering or defects in the experimental samples, but our results finally resolve the large disparity between the theoretically calculated and experimentally measured magnetic anisotropy of $IrMn_3$. We note that, although the energy surface illustrated in Fig. 2(a) has an unusually complex form, the minima themselves exhibit a fourfold symmetry, characteristic of cubic rather than uniaxial anisotropy. The question remains how to resolve the apparent contradiction with the experimental data of Vallejo-Fernandez *et al.* [17] and its requirement of a magnetization scaling exponent consistent with uniaxial symmetry.

To resolve this discrepancy, we now investigate the temperature dependence of the anisotropy constant to calculate the scaling exponent. The energy surfaces and minimum energy path were calculated for temperatures between 0 K and 350 K as shown in Fig. 3(a). The absolute free energy increases with temperature due to spin fluctuations but the free-energy barrier between neighboring ground-state minima, i.e., the magnetic anisotropy, decreases. In Fig. 3(b), we plot the power-law dependence of the effective energy barrier as a function of the magnetization and find an unusual exponent of $l = 3.92, \pm 0.14$. The exponent is closer to a uniaxial exponent of $l = 3$, matching the experimental observations but deviates from this ideal value due to the complex symmetry of the anisotropy energy surface. We also note that the specific scaling exponent is dependent on the strength of the anisotropy, and for weaker anisotropy tends towardan exponent of $l = 3$, which may be seen in similar noncollinear magnets such as $PtMn_3$. We conclude that the magnetic anisotropy of $L1_2$-$IrMn_3$ possesses a close to uniaxial temperature dependence in direct contradiction with the usual Callen-Callen power laws and cubic nature of the crystal [11].

Finally, another problem in calculating the anisotropy comes from the experimentally determined values of the anisotropy constant; we consider the basis of the experiments [17,18], where the attempt frequency f_0 is a critical parameter in calculating the effective anisotropy. Having determined the precise energy barrier at an elevated temperature, we are now able to compute the attempt frequency using atomistic spin dynamics. We simulate the dynamic behavior using the stochastic Landau-Lifshitz-Gilbert (sLLG) equation [24,27]

$$\frac{\partial \mathbf{S}_i}{\partial t} = -\frac{\gamma}{1+\lambda^2}[\mathbf{S}_i \times \mathbf{B}_{\text{eff}} + \lambda \mathbf{S}_i \times (\mathbf{S}_i \times \mathbf{B}_{\text{eff}})], \quad (5)$$

where λ is the Gilbert damping constant and $|\gamma|$ is the gyromagnetic ratio. The effective field $\mathbf{B}_{\text{eff}}$ is calculated as the derivative of the spin Hamiltonian with respect to the local spin moment plus a random thermal field ($\mathbf{B}_{\text{eff}} = -\mu_S{}^{-1}\partial\mathscr{H}/\partial\mathbf{S}_i + \mathbf{B}^i_{\text{th}}$), where $\mathbf{B}^i_{\text{th}} = \Gamma(t)\sqrt{\frac{2\lambda k_B T}{\gamma \mu_S \Delta t}}$ and Γ is a 3D random Gaussian distribution. The sLLG equation is integrated using a second-order predictor corrector Heun scheme [24].

We determined the attempt frequency by calculating the transition rate just below the blocking temperature of the antiferromagnet. Due to the giant anisotropy of $IrMn_3$ and limited time accessible by simulations, we simulate a small sample $(1.5\ \text{nm})^3$ which has a blocking temperature of $T_B = 101.5$K for a timescale of 0.1 ns. To precisely calculate the energy barrier for this system at 100 K, we use the same method as above to calculate the energy surface. The time-dependent dynamics of the magnetization for a single sublattice is shown in Fig. 4.

As the temperature is just below the blocking temperature, the IrMn switches between stable states giving a time-dependent form similar to telegraph noise. Over a total simulation time of 100 ns, the total number of transitions was calculated and divided by the total simulation time. The frequency of the transitions is dependent on the magnitude of the damping constant, which is typically in the range 0.01 to 1 for materials with large spin-orbit coupling. The simulation was repeated for damping constants within this range to determine the variation in the attempt frequency, giving f_0 values between 0.1 and 4×10^{12} Hz, shown in Fig. 4. The simulated values are of the same order as the experimentally determined value [19] and provide reasonable bounds for the attempt frequency for noncollinear antiferromagnets.

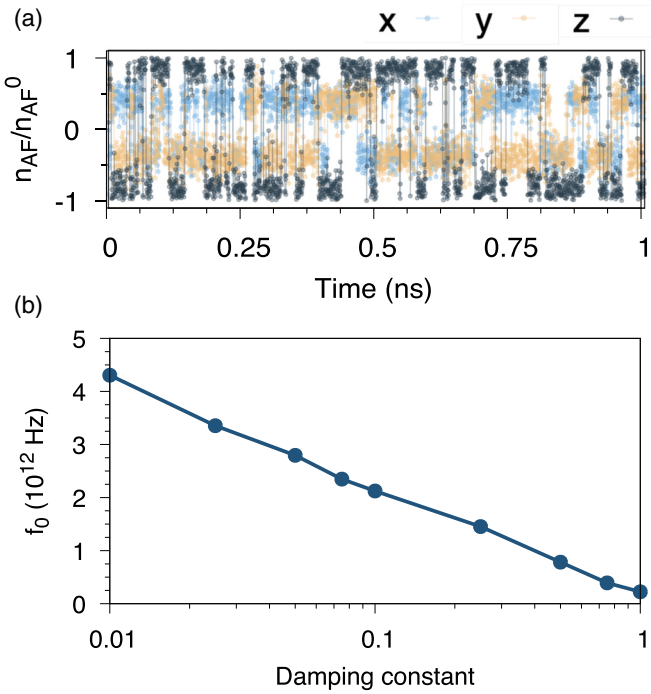

FIG. 4. Time-dependent magnetization of $IrMn_3$ at 100 K simulated using atomistic spin dynamics and dependence of the switching frequency on the damping constant. (a) The magnetization of IrMn was simulated for 100 ns for a damping constant of 0.1, where only the first 1 ns is shown for clarity. The sublattice magnetization flips superparamagnetically between different coherent ground-state orientations. At this temperature, the sublattice ordering is approximately 90% since the system is simulated far from the Néel temperature. (b) Dependence of the attempt frequency for reasonable values of the damping constant from 0.01–1 shows a range for the attempt frequency between $f_0 = 0.1 - 4$ THz

IV. DISCUSSION

Applying constrained minimization and spin dynamics simulations, we have determined the symmetry and effective temperature-dependent anisotropy and relaxation dynamics of $IrMn_3$, one of the most technologically important noncollinear AF materials. We find that the anisotropy energy surface is unusually complex and find a scaling exponent of the effective magnetic anisotropy that is fundamentally different from the expectations of Callen-Callen theory despite the presence of cubic crystal symmetry and localized uniaxial anisotropy at atomic Mn sites. Metastable spin structures are shown to lower the overall energy barrier to a tenth of that estimated from simple geometrical approximations. Spin dynamics calculations reveal an exceptionally high attempt frequency in $IrMn_3$ of between $f_0 = 0.1$ and 4×10^{12} s^{-1}; a value three orders of magnitude larger than the typical value chosen for ferromagnets of 10^9 s^{-1}. Considering a specific value for the damping constant of $\lambda \approx 0.1$ gives a comparable value of the attempt frequency with respect to the measured experimental value [19] of 2.4 THz. We have therefore resolved the outstanding discrepancy between theory and experiments calculating a value for the anisotropy energy within 10% of the experimental value.

From the structure of the zero Kelvin energy surface we conclude that the magnetic anisotropy of $L1_2$- $IrMn_3$ possesses a unique symmetry not seen for ferromagnets, yet consistent with the expected relationship to the crystal symmetry by rotation of the ground-state spin structure. We find that the scaling of the anisotropy is similarly unusual with an exponent of 3.92, which is closer to uniaxial magnetization scaling of the anisotropy despite the near-cubic symmetry. The resolution of this apparent contradiction (and the associated experimental measurements) is as follows. Although the anisotropy is shown to have cubiclike symmetry, the scaling arises from the spin fluctuations which reflect the local uniaxial environment of individual spins. This is an intriguing and unusual separation of the fundamental origin of the MAE and the temperature dependence of the anisotropy.

Although we have focused on $IrMn_3$ we expect that other noncollinear antiferromagnets such as MnPt and MnFe will exhibit similarly complex temperature-dependent magnetic anisotropy. This is likely to be strongly affected by composition and ordering which will disrupt the local anisotropy energy surface at different atomic sites. Our results have important consequences for applications of antiferromagnets in determining their thermal stability and dynamic properties and provide an established methodology for determining the effective magnetic anisotropy at elevated temperatures. This is particularly important for emerging applications in neuromorphic computing and AF spintronics where the long-term stability of the antiferromagnet is critical to device operation. Further investigation may yield different classes of antiferromagnets with unusual temperature-dependent properties.

ACKNOWLEDGMENTS

We gratefully acknowledge the provision of computer time made available on the VIKING cluster, a high performance compute facility provided by the University of York. Financial support of Seagate Technology is gratefully acknowledged.

[1] P. Wadley, B. Howells, J. elezny, C. Andrews, V. Hills, R. P. Campion, V. Novak, K. Olejnik, F. Maccherozzi, S. S. Dhesi, S. Y. Martin, T. Wagner, J. Wunderlich, F. Freimuth, Y. Mokrousov, J. Kune, J. S. Chauhan, M. J. Grzybowski, A. W. Rushforth, K. W. Edmonds, B. L. Gallagher, and T. Jungwirth, Electrical switching of an antiferromagnet, Science **351**, 587 (2016).

[2] T. Jungwirth, J. Sinova, A. Manchon, X. Marti, J. Wunderlich, and C. Felser, The multiple directions of antiferromagnetic spintronics, Nat. Phys. **14**, 200 (2018).

[3] T. Jungwirth, X. Marti, P. Wadley, and J. Wunderlich, Antiferromagnetic spintronics, Nat. Nanotechnol. **11**, 231 (2016).

[4] M. Meinert, D. Graulich, and T. Matalla-Wagner, Electrical switching of antiferromagnetic Mn_2Au and the role of thermal activation, Phys. Rev. Appl. **9**, 064040 (2018).

[5] P.-H. Lin, B.-Y. Yang, M.-H. Tsai, P.-C. Chen, K.-F. Huang, H.-H. Lin, and C.-H. Lai, Manipulating exchange bias by spin-orbit torque, Nat. Mater. **18**, 335 (2019).

[6] W. H. Meiklejohn and C. P. Bean, New magnetic Anisotropy, Phys. Rev. **105**, 904 (1957).

[7] K. O'Grady, L. E. Fernandez-Outon, and G. Vallejo-Fernandez, A new paradigm for exchange bias in polycrystalline thin films, J. Magn. Magn. Mater. **322**, 883 (2010).

[8] J. Nogués and I. K. Schuller, Exchange bias, J. Magn. Magn. Mater. **192**, 203 (1999).

[9] D. Ielmini, Brain-inspired computing with resistive switching memory (RRAM): Devices, synapses and neural networks, Microelectron. Eng. **190**, 44 (2018).

[10] C. Zener, Classical theory of the temperature dependence of magnetic anisotropy energy, Phys. Rev. **96**, 1335 (1954).

[11] H. B. Callen and E. Callen, The present status of the temperature dependence of magnetocrystalline anisotropy, and the l(l+1)2 power law, J. Phys. Chem. Solids **27**, 1271 (1966).

[12] A. Kohn, A. Kovács, R. Fan, G. J. McIntyre, R. C. C. Ward, and J. P. Goff, The antiferromagnetic structures of $IrMn_3$ and their influence on exchange-bias, Sci. Rep. **3**, 2412 (2013).

[13] I. Tomeno, H. N. Fuke, H. Iwasaki, M. Sahashi, and Y. Tsunoda, Magnetic neutron scattering study of ordered Mn_3Ir, J. Appl. Phys. **86**, 3853 (1999).

[14] L. Szunyogh, B. Lazarovits, L. Udvardi, J. Jackson, and U. Nowak, Giant magnetic anisotropy of the bulk antiferromagnets IrMn and $IrMn_3$ from first principles, Phys. Rev. B **79**, 020403(R) (2009).

[15] L. Szunyogh, L. Udvardi, J. Jackson, U. Nowak, and R. Chantrell, Atomistic spin model based on a spin-cluster expansion technique: Application to the $IrMn_3$ /Co interface, Phys. Rev. B **83**, 024401 (2011).

[16] M. Tsunoda, S. Yoshitaki, Y. Ashizawa, C. Mitsumata, T. Nakamura, H. Osawa, T. Hirono, D. Y. Kim, and M. Takahashi, Uncompensated antiferromagnetic spins at the interface in Mn-Ir based exchange biased bilayers, J. Appl. Phys. **101**, 09E510 (2007).

[17] G. Vallejo-Fernandez, L. E. Fernandez-Outon, and K. O'Grady, Measurement of the anisotropy constant of antiferromagnets in metallic polycrystalline exchange biased systems, Appl. Phys. Lett. **91**, 212503 (2007).

[18] R. Carpenter, A. J. Vick, A. Hirohata, G. Vallejo-Fernandez, and K. O'Grady, Effect of grain cutting in exchange biased nanostructures, J. Appl. Phys. **115**, 17B905 (2014).

[19] G. Vallejo-Fernandez, N. P. Aley, J. N. Chapman, and K. O'Grady, Measurement of the attempt frequency in antiferromagnets, Appl. Phys. Lett. **97**, 222505 (2010).

[20] B. Craig, R. Lamberton, A. Johnston, U. Nowak, R. W. Chantrell, and K. O'Grady, A model of the temperature dependence of exchange bias in coupled ferromagnetic/antiferromagnetic bilayers, J. Appl. Phys. **103**, 07C102 (2008).

[21] S. Jenkins and R. F. L. Evans, Enhanced finite size and interface mixing effects in iridium manganese ultra thin films, J. Appl. Phys. **124**, 152105 (2018).

[22] L. Neel, L'approche à la saturation de la magnétostriction, J. Phys. Radium **15**, 376 (1954).

[23] J. D. Alzate-Cardona, D. Sabogal-Suárez, R. F. L. Evans, and E. Restrepo-Parra, Optimal phase space sampling for Monte Carlo simulations of Heisenberg spin systems, J. Phys.: Condens. Matter **31**, 095802 (2019).

[24] R. F. L. Evans, W. J. Fan, P. Chureemart, T. A. Ostler, M. O. A. Ellis, and R. W. Chantrell, Atomistic spin model simulations of magnetic nanomaterials, J. Phys.: Condens. Matter **26**, 103202 (2014).

[25] VAMPIRE software package v5 available from https://vampire.york.ac.uk (2019).

[26] P. Asselin, R. F. L. Evans, J. Barker, R. W. Chantrell, R. Yanes, O. Chubykalo-Fesenko, D. Hinzke, and U. Nowak, Constrained Monte Carlo method and calculation of the temperature dependence of magnetic anisotropy, Phys. Rev. B **82**, 054415 (2010).

[27] M. O. A. Ellis, R. F. L. Evans, T. A. Ostler, J. Barker, U. Atxitia, O. Chubykalo-Fesenko, and R. W. Chantrell, The Landau-Lifshitz equation in atomistic models, Low Temp. Phys. **41**, 705 (2015).